Chromatin accessibility landscapes activated by cell-surface and intracellular immune receptors

Pingtao Ding[1,7,*], Toshiyuki Sakai[1], Ram Krishna Shrestha[1], Nicolas Manosalva Perez[2,3], Wenbin Guo[4], Bruno Pok Man Ngou[1], Shengbo He[5], Chang Liu[6], Xiaoqi Feng[5], Runxuan Zhang[4], Klaas Vandepoele[2,3], Dan MacLean[1], Jonathan DG Jones[1,*]

1 The Sainsbury Laboratory, University of East Anglia, Norwich Research Park, Norwich NR4 7UH, United Kingdom

2 Department of Plant Biotechnology and Bioinformatics, Ghent University, Technologiepark 71, 9052 Ghent, Belgium

3 VIB Center for Plant Systems Biology, Technologiepark 71, 9052 Ghent, Belgium

4 Information and Computational Sciences, The James Hutton Institute, Dundee DD2 5DA, United Kingdom

5 John Innes Centre, Norwich Research Park, Norwich NR4 7UH, United Kingdom

6 Institute of Biology, University of Hohenheim, Garbenstrasse 30, 70599 Stuttgart, Germany

7 Current Address: Institute of Biology Leiden, Leiden University, Sylviusweg 72, Leiden 2333 BE, The Netherlands

* For correspondence: p.ding@biology.leidenuniv.nl (lead contact); jonathan.jones@tsl.ac.uk

ORCiD of authors:

PD: 0000-0002-3535-6053; TS: 0000-0003-2737-3299; RKS: 0000-0001-5542-6269; WG: 0000-0002-1829-6044; BN: 0000-0002-0760-1058; SH: 0000-0003-3773-9995; CL: 0000-0003-2859-4288; XF: 0000-0002-4008-1234; RZ: 0000-0001-7558-765X; KV: 0000-0003-4790-2725; DM: 0000-0003-1032-0887; JDGJ: 0000-0002-4953-261X

Twitter handles of first author and corresponding

PD: @sardineboy_DING; JDGJ: @jonathandgjones

Highlight

Effective plant immunity requires activation of both cell-surface and intracellular receptors. Here, Ding et al. (2021) have applied methods that reveal induced open chromatin to unravel novel gene regulatory mechanisms during this process.

Abstract

Activation of cell-surface and intracellular receptor-mediated immunity results in rapid transcriptional reprogramming that underpins disease resistance. However, the mechanisms by which co-activation of both immune systems lead to transcriptional changes are not clear. Here, we combine RNA-seq and ATAC-seq to define changes in gene expression and chromatin accessibility. Activation of cell-surface or intracellular receptor-mediated immunity, or both, increases chromatin accessibility at induced defense genes. Analysis of ATAC-seq and RNA-seq data combined with publicly available information on transcription factor DNA-binding motifs enabled comparison of individual gene regulatory networks activated by cell-surface or intracellular receptor-mediated immunity, and by both. These results and analyses reveal overlapping and conserved transcriptional regulatory mechanisms between the two immune systems.

3

Introduction

Plants use both cell-surface and intracellular receptors to detect pathogen-derived molecules and activate innate immunity (Jones and Dangl, 2006). Plant cell-surface immune receptors (pattern recognition receptors, or PRRs) perceive relatively conserved pathogen-associated molecular patterns (PAMPs) or endogenous damage-associated molecular patterns (DAMPs) released from damaged or dying plant cells and activate Pattern- or DAMP-triggered immunity (PTI or DTI) (Choi and Klessig, 2016; Bacete *et al.*, 2018). Intracellular immune receptors in plants are usually nucleotide-binding, leucine-rich repeat (NLR) proteins. NLRs recognize, directly or indirectly, pathogen effectors secreted into plant cells and activate effector-triggered immunity (ETI). These innate immune systems involve distinct responses mediated by different subsets of molecular components (Ngou *et al.*, 2020*a*). Some cell-surface receptors, such as tomato Cf-4 and Cf-9 detect apoplastic effectors yet activate both PTI-like and ETI-like responses (Hammond-Kosack and Jones, 1997). The main fundamental distinction is between processes initiated by cells-surface or intracellular immune receptors (Supplementary Fig. 1). In interactions between plants and microbial pathogens, PTI will always precede ETI, since effector delivery requires intimate host/microbe contact.

We study the Arabidopsis RPS4/RRS1 NLR pair as a model to study ETI, which detects bacterial effectors AvrRps4 and PopP2. Using a *Pseudomonas* strain that solely delivers one of these effectors, we defined early RPS4/RRS1-dependent transcriptional responses in Arabidopsis leaves (Sohn *et al.*, 2014; Ding *et al.*, 2020), and showed that 4 hours after infiltration, PTI together with ETI ('PTI+ETI') elevates the expression of defense-related genes more strongly compared to PTI alone (Sohn *et al.*, 2014; Ding *et al.*, 2020). This early timepoint precedes accumulation of defense hormone salicylic

4

acid (SA) and gene reprogramming in response to increased endogenous SA level (Sohn *et al.*, 2014; Ding *et al.*, 2020). This implies that ETI-enhanced transcriptional regulation plays an essential role in conferring robust immune responses against pathogens (Ngou *et al.*, 2020*a*), but how ETI activates defense genes remains unclear. To study ETI-specific physiological changes, we generated an inducible ETI system (Ngou *et al.*, 2020*b*).

Activation of PTI, ETI and 'PTI+ETI' lead to rapid transcriptional reprogramming (Sohn *et al.*, 2014; Hillmer *et al.*, 2017; Ding *et al.*, 2020). Many transcriptional regulatory components are known to be involved in orchestrating effective immunity in plants (Tsuda and Somssich, 2015; Li *et al.*, 2016), notably transcription factors (TFs) (Zhang *et al.*, 2010), transcription co-repressors (Zhu *et al.*, 2010), the Mediator complex (Kidd *et al.*, 2009), histone-modifying enzymes (Zhou *et al.*, 2005), and histone remodellers (Walley *et al.*, 2008). Little is known of how changes in transcription rates at defense genes are initiated, maintained and regulated upon the activation of either class of plant immune receptor.

Open Accessible Chromatin Regions (ACRs) at promoters and enhancers are associated with active gene expression in eukaryotes (Tsompana and Buck, 2014). DNA methylation, histone deacetylation, and histone methylation can prime the promoters of immune-related genes required for disease defense (Chen *et al.*, 2017). Conversion between "closed" and "open" chromatin states results from the chromatin remodeling, which is regulated by multiunit complexes. Several putative chromatin remodelers play important roles in regulating defense gene expression during the activation of PTI and ETI, including the SWI/SNF chromatin remodeler SYD (SPLAYED) (Johnson *et al.*, 2015), the SWR1c subunits PHOTOPERIOD-INDEPENDENT EARLY FLOWERING1 (PIE1), ACTIN-RELATED PROTEIN6 (ARP6), and SWR1 COMPLEX 6 (SWC6), as well as H2A.Z (Berriri *et al.*, 2016), and the CHROMATIN-REMODELING FACTOR 5 (CHR5) (Zou *et al.*, 2017). However, the detailed profiling of

chromatin status induced by PTI, ETI or 'PTI+ETI' has never been reported before, and the direct association between the changes in the chromatin status and the changes in defense gene expression is unclear.

Applications of assays for transposase-accessible chromatin following by sequencing (ATAC-seq) in plants have revealed species-, tissue- and cell-type-specific chromatin signatures in recent studies (Lu *et al.*, 2017, 2019; Maher *et al.*, 2018; Potter *et al.*, 2018; Frerichs *et al.*, 2019), but chromatin accessibility changes associated with inducible responses and environmental perturbations, such as immune activation are less well characterized. We hypothesized that correlating immunity-specific transcriptomes with an atlas of open chromatin profiles could reveal *cis*-regulatory elements (CREs) and associated regulatory mechanisms that underpin these changes. We therefore performed a set of comparative analyses with ATAC-seq and RNA-seq data generated during PTI, 'PTI+ETI' and ETI. This study provides an extensive data resource to the plant-microbe interaction community, which demonstrates a direct link between changes in chromatin accessibility and associated gene expression and new insights into the dynamics of chromatin accessibility landscapes and gene regulatory networks during plant immune activation.

Materials and methods

Plant materials and growth condition. *Arabidopsis thaliana* Columbia-0 (Col-0) accession was used as wild type in this study. SETI[WT] and SETI[mut] transgenic plants used have been described previously (Ngou *et al.*, 2020*b*). Seeds were sown on compost and plants were grown at 21 °C with 10 hours under light and 14 hours in dark, and at 70% humidity. The light level is approximately 180-200 µmols with fluorescent tubes.

Activation of PTI and 'PTI+ETI'. *Pseudomonas fluorescens* engineered with a type III secretion system (Pf0-1 'EtHAn' strains) expressing one of wild-type AvrRps4 or AvrRps4 KRVY135-138AAAA mutant effectors were grown on selective KB plates for 24 h at 28 °C (Thomas *et al.*, 2009; Sohn *et al.*, 2014). Bacteria were harvested from the plates, resuspended in infiltration buffer (10 mM MgCl$_2$) and the concentration was adjusted to OD$_{600}$ = 0.2 (10^8 CFU•mL^{-1}). The abaxial surfaces of 5-week-old Arabidopsis leaves were hand infiltrated with a 1-mL disposable needleless syringe (Slaughter Ltd, R & L, catalogue number: BS01T). Leaves infiltrated with 10 mM MgCl$_2$ serves as mock treatment. Leaves infiltrated with Pf0-1:AvrRps4^{WT} activates 'PTI+ETI', and those infiltrated with Pf0-1:AvrRps4^{mut} activates PTI only (Ngou *et al.*, 2020*a*).

Activation of ETI. 5-week-old Arabidopsis leaves of SETI^{WT} (E2:AvrRps4^{WT}) infiltrated with 50 μM β-estradiol (E2, Sigma-Aldrich, catalogue number: E8875; dissolved in 100% dimethyl sulfoxide, also known as DMSO, Sigma-Aldrich, catalogue number: D8418) activates 'ETI' only, as described previously(Ngou *et al.*, 2020*b*). 0.1% DMSO (same titrate as 50 mM E2 stock solution diluted in pure water and generating 50 μM E2 working solution) in pure water used as mock treatment for infiltration with a 1-mL needleless syringe. SETI^{mut} (E2:AvrRps4^{mut}) with similar treatments as in SETI^{WT} serve as additional negative ETI controls, as described previously (Ngou *et al.*, 2020*b*).

RNA isolation and sequencing (RNA-seq). Leaf samples from PTI, 'PTI+ETI', ETI were isolated as described previously (Ding *et al.*, 2020). Total RNA samples are sent by dry ice to BGI for mRNA isolation and library construction and sequenced on BGISEQ-500 sequencing platforms.

RNA-seq raw data processing, alignment and quantification of expression and data visualization. Raw reads are trimmed into clean reads by BGI bioinformatic service into 50 bp. At least 12 million single-end clean reads for each sample were provided by BGI for RNA-seq analysis. All reads have passed FastQC before the following analyses (Simon Andrews; FastQC: https://www.bioinformatics.babraham.ac.uk/projects/fastqc/). All clean reads are either mapped to TAIR10 Arabidopsis genome/transcriptome via TopHat2 or to a comprehensive Reference Transcript Dataset for Arabidopsis (AtRTD2) containing 82,190 non-redundant transcripts from 34,212 genes via Kallisto (PTI and 'PTI+ETI') or Salmon (ETI) tools (Kim *et al.*, 2013; Bray *et al.*, 2016; Patro *et al.*, 2017; Zhang *et al.*, 2017). Detailed scripts and versions of each software can be found via the GitHub link: https://github.com/TeamMacLean/fastqc_kallisto_analysis. Mapped reads were sorted with SAMtools and visualized in Integrative Genomics Viewer (IGV) with TAIR10 reference genome (Li *et al.*, 2009; Robinson *et al.*, 2011; Kim *et al.*, 2013). The estimated gene transcript counts were used for differential gene expression analysis, statistical analysis and data through the 3D RNA-seq software (Guo *et al.*, 2020). For both datasets, the low expressed transcripts were filtered if they did not meet the criteria ≥ 3 samples with ≥ 1 count per million reads (CPMs). An expressed gene must have at least one expressed transcript. The batch effects between biological replicates were removed to reduce artificial variance with RUVSeq method (Risso *et al.*, 2014). The expression data was normalized across samples with TMM method (Robinson and Oshlack, 2010). The significance of expression changes in the contrast groups 'PTI vs no treatment' and 'PTI+ETI vs no treatment', and 'ETI vs Control_1' and 'ETI vs ETI_mut' were determined by the limma-voom method (Law *et al.*,

8

2014; Ritchie *et al.*, 2015). A gene was defined as significant DEG if the BH adjusted p-value < 0.01 and $\log_2(\text{fold\_change}) \geq 1$.

FANS-ATAC-seq. Leaf samples from PTI, 'PTI+ETI', ETI and control conditions were collected at 4 hpi of treatment (same time points as RNA-seq samples) or without any treatment. 2 fully expanded leaves with treatment from each plant and 3 plants in total are collected as one sample and one biological replicate. 6 leaves of one sample were chopped quickly in 1 mL 4-°C-prechilled phosphate-buffered saline (PBS) buffer (1×, pH 7.4) with a clean unused razor blade (Agar Scientific Ltd, catalogue number: T586) into fine pieces (less than 1 min). The leaf lysis containing crude nuclei extract was transferred and filtered through a 30-μm CellTrics® cell strainer (Sysmex, catalogue number: 04-0042-2316) into a 100×16-mm round-base test tube (Slaughter Ltd, R & L, catalogue number: 142AS) with 1-mL sterile tip by pipetting. The sharp end of the tip was cut off and shortened with 2-mm in length by a pair of sterile scissors to minimize the damage to the nuclei. All samples of leaf lysis were kept on ice immediately after the transfer. 1-mL CyStain PI Absolute P nuclei 4',6-diamidino-2-phenylindole (DAPI) staining buffer (Sysmex, catalogue number: 05-5022) was added into each nuclei extract. Nuclei extract with the staining buffer were gently mix and kept on ice. Stained nuclei extract were submitted to BD FACSMelody Cell Sorter with a green laser for fluorescence-assisted nuclei sorting (FANS) with a similar setting as described previously (Lu *et al.*, 2017). FANS-purified nuclei samples were collected in 1.5 DNA LoBind Eppendorf microcentrifuge tubes (Fisher Scientific, catalogue number: 10051232) and kept on ice. Nuclei pellets were collected as described previously by centrifugation at 1,000 × *g* and tagmented with Nextera DNA Library Prep Kit (Illumina, catalog number: FC-121-1030, now discontinued; replacement can be found as Illumina Tagment DNA TDE1 Enzyme and Buffer Kits, catalog numbers: 20034197 or 20034198) (Buenrostro *et al.*, 2015). We used 0.1 μL TDE1 enzyme in a 5 μl total reaction mix for each ATAC samples. The following PCR library construction and quality control steps were performed as recommended

9

(Buenrostro *et al.*, 2015). The only difference here was that we used dual index primers designed by ourselves for barcoding the libraries and multiplexing. Those primers have been validated in our previous experiments (Ding *et al.*, 2020), and the detailed sequence information can be found in Supplementary Table 1. Multiplexed ATAC-seq libraries were sequenced with multiple NextSeq 500/550 High Output Kits (75 Cycles) on an in-house NextSeq 550 sequencer.

ATAC-seq raw data processing and alignment. Sequencing results were demultiplexed using bcl2fastq tool to generate adaptor-trimmed raw reads. Pair-end and 37 bp each end reads were tested with FastQC and Picard tools for quality control and testing PCR duplications. Raw reads were mapped to TAIR10 Arabidopsis reference genome with Bowtie2 and sorted with SAMtools (Li *et al.*, 2009; Langmead and Salzberg, 2012). Reads mapped to chloroplast and mitochondria were removed before the follow-up analyses. Detailed scripts, software versions and QC outputs can be found in the GitHub link: https://github.com/TeamMacLean/dingp_atacseq_for_publication.

Identification of ACRs. Identification of ACRs was done by callpeak function in MACS v.2.2.7(Zhang *et al.*, 2008). All replicates of samples under specific condition were used as input of treatment and genomic DNA samples were used as input of control. For visualization of fold enrichment of mapped reads compared control samples, FE.bdg files were generated by bdgcmp function in MACS. FE.bdg files were visualized by IGV(Robinson *et al.*, 2011). In the trial analysis of FANS-ATAC-seq, we counted mapped reads for ACRs using coverage function in Bedtools v.2.28.0 (Quinlan and Hall, 2010). Then, we made correlation plots based on log2 read counts of each common ACR between replicates to find out the reproducibility for 10k, 20k, 50k, and 80k samples using our R script, which is listed in our GitHub link: https://github.com/slt666666/Plant_Innate_Immunity_ATAC-seq.

10

Profile of ACRs binding to TSS/TTS regions. The heatmap of ACRs binding to TSS regions and the distribution of ACRs binding to TSS and TTS regions were obtained by ChIPSeeker v.1.24.0 package within R (Yu *et al.*, 2015). The features of ACRs were annotated by ChIPSeeker package using the annotatePeak function. In this part, promoters were defined as -2,000 to 1,000 bp from the TSS. The Upset plot which showed ACRs shared on several conditions were generated by UpSetR package based on the nearest genes from ACRs (Conway *et al.*, 2017).

Identification of DARs. Identification of DARs is achieved by applying callpeak function of MACS. All replicates of samples under specific condition were used as input of treatment and all replicates of samples under corresponding control conditions were used as input of control. Annotation of genes with enriched DARs within 2 kb upstream of a gene is done by annotatePeakInBatch function in ChIPpeakAnno package (Yu *et al.*, 2015). Annotation of genes with the other DARs in distal intergenic genome loci is done by our Python script.

Integration of DEGs and DARs. The identification of common genes to annotated genes with enriched DARs and significantly upregulated (log2FC > 1, q-value < 0.01) genes is done by our Python script. The GO analysis for these common genes is conducted by g:Profiler (Raudvere *et al.*, 2019). All scripts used for the analyses of ACRs and integration of DEGs and DARs are available: https://github.com/slt666666/Plant_Innate_Immunity_ATAC-seq.

Motif-based inference of gene regulatory networks using ACRs. The inference of GRNs was done using an ensemble motif mapping method described previously (Kulkarni *et al.*, 2019), combining all the matches from Find Individual Motif Occurrences (FIMO) with the top 7000 matches from Cluster-Buster (CB) (Frith *et al.*, 2003; Grant *et al.*, 2011). This mapping information was used to determine which motifs were significantly enriched in the ACRs derived from the ATAC-seq experiments for

11

each condition (PTI, ETI and 'PTI+ETI'). Per condition, for TFs showing differential expression the associated motifs were tested for enrichment in the ACRs and significant motifs were retained (adjusted p-value ≤ 0.01). Based on motif coordinates in ACRs, individual motif matches were assigned to the closest gene, establishing a link between the TFs that bind these motifs and putative target genes. The differential expression information was integrated to identify only the TFs and target genes that were differentially expressed for each condition. Finally, for each TF, the putative target genes set was analyzed for over-represented GO Biological Process terms (only using experimentally and curated annotations; hypergeometric distribution q-value < 0.001).

Results

ATAC-seq in Arabidopsis reveals tissue-specific chromatin accessibility

ATAC-seq was first used to capture open chromatin regions in human cell lines and rapidly adapted to other eukaryotic systems including plants (Buenrostro *et al.*, 2013; Lu *et al.*, 2017). To study the dynamic chromatin features during plant immune activation, we established a protocol to prepare fresh nuclei isolated from adult rosette leaves of Arabidopsis (*Arabidopsis thaliana*) Columbia-0 (Col-0) ecotype using fluorescence-activated nuclei sorting (FANS) (Supplementary Fig. 2a). A similar approach was reported previously (Lu *et al.*, 2017). To generate FANS-ATAC-seq libraries from multiple samples that are (i) compatible with the Illumina next-generation sequencing (NGS) sequencing platforms and (ii) can be multiplexed we designed and synthesized barcoded primers with 9-nucleotide (nt) unique indices for dual index and paired-end sequencing (Supplementary Fig. 2b-d; Supplementary Table 1). In a trial run we used 10,000 (10k), 20k, 50k and 80k sorted nuclei as ATAC input with a fixed amount of 'tagmentation' reaction, to obtain an optimal ratio between the input nuclei (DNA) and Tn5 transposase (Supplementary Fig. 3a). Purified naked Arabidopsis genomic DNA was tagmented in three replicates and sequenced as controls for ATAC-seq

12

normalization (Supplementary Fig. 2d). In this trial FANS-ATAC-seq run, we observed reproducible accessible chromatin features captured in two biological replicates with different levels of input (Supplementary Fig. 3b-e).

To test if this ATAC-seq method is sensitive enough to detect tissue-specific chromatin accessible features, we additionally performed FANS-ATAC-seq with sperm nuclei (SN) and vegetative nuclei (VN), the male germ unit derived from Arabidopsis pollen grain. We found that ACRs enriched at the *SYSTEMIC ACQUIRED RESISTANCE DEFICIENT 1* (*SARD1*) defense gene locus are only observed in somatic but not germline cells (Supplementary Fig. 4a). *SARD1* encodes a TF involved in plant immunity (Zhang *et al.*, 2010; Wang *et al.*, 2011; Sun *et al.*, 2015). We inspected another well-known *Resistance* (*R*)-gene cluster on Arabidopsis chromosome 4 which harbors a group of N-terminal Toll/interleukin-1 receptor/resistance protein (TIR) domain-containing NLRs. Similar to *SARD1*, promoters of the NLR-encoding genes *RECOGNITION OF PERONOSPORA PARASITICA 4* (*RPP4*) or *CHILLING SENSITIVE 2* (*CHS2*), *SUPPRESSOR OF NPR1-1, CONSTITUTIVE 1* (*SNC1*), *SIDEKICK SNC1 1* (*SIKIC2*) and *RESISTANCE TO LEPTOSPHAERIA MACULANS 3* (*RLM3*) show enriched ACRs in leaf nuclei ATAC-seq data compared to the other four *NLRs* in the same gene cluster, but not in SN or VN ATAC-seq data (Supplementary Fig. 4b). This is consistent with the observation that expression levels of *RPP4/CHS2*, *SNC1*, *SIKIC2* and *RLM3* in Arabidopsis adult leaves are much higher than the other four NLRs in the same gene cluster (Schmid *et al.*, 2005). Expression of *RPP4/CHS2*, *SNC1*, *SIKIC2* and *RLM3* in Arabidopsis leaves contributes to resistance against multiple pathogens (van der Biezen *et al.*, 2002; Zhang *et al.*, 2003; Staal *et al.*, 2008; Dong *et al.*, 2018; Asai *et al.*, 2018). In addition, trimethylations of the 4th lysine of the histone H3 (H3K4me3s), histone marks that are often associated with actively transcribed genes, is enriched in *RPP4/CHS2* and *SNC1* promoters in Arabidopsis (Xia *et al.*, 2013), supporting our ATAC-seq results (Supplementary Fig. 4b). Overall, ACRs enriched in immunity-related genes are specific to somatic but not to germline cells.

13

ATAC-seq to study Arabidopsis inducible innate immunity

We applied the FANS-ATAC-seq method to study changes in chromatin accessibility associated with gene expression induced by innate immunity. In Arabidopsis Col-0, two paired NLR proteins RPS4/RRS1 and RPS4B/RRS1B serve as intracellular NLR receptors activating ETI upon recognition of AvrRps4, an effector derived from *Pseudomonas* (*P.*) *syringae* pv. *pisi*, a causal agent of bacterial blight in pea (*Pisum sativum*) (Saucet *et al.*, 2015). We use a non-pathogenic strain of *P. fluorescens* Pf0-1 engineered with the type III secretion system (T3SS) from *P. syringae* ('Effector-to-Host Analyzer' or EtHAn) as a tool to deliver wild-type AvrRps4 (Pf0-1:AvrRps4[WT]) or its mutant (Pf0-1:AvrRps4[mut]) into Col-0 leaf cells (Sohn *et al.*, 2009; Thomas *et al.*, 2009). AvrRps4[mut] (KRVY135-138AAAA) is unable to activate ETI mediated by RPS4/RRS1 and RPS4B/RRS1B (Saucet *et al.*, 2015). Infiltration of Pf0-1:AvrRps4[mut] activates PTI, and Pf0-1:AvrRps4[WT] activates 'PTI+ETI' (Supplementary Fig. 5a), as in previous reports (Ding *et al.*, 2020; Ngou *et al.*, 2021). We took samples at 4 hours post-infiltration (hpi) for ATAC-seq to monitor early changes during immune activation (Supplementary Fig. 5a) (Sohn *et al.*, 2014; Ding *et al.*, 2020). We obtained similar patterns of genome-wide ATAC-seq peak coverage with different treatments (Supplementary Fig. 5b).

ATAC-seq peaks in all biological replicates under different conditions were enriched within 2 kilobases (kb) upstream of the transcription start site (TSS) and within 1 kb downstream of the transcript termination site (TTS) (Fig. 1a,b). The distribution of ACRs relative to genomic features was highly similar between all ATAC-seq data sets (Supplementary Fig. 5c-f; Supplementary Table 2). Over 77% of ACRs are mapped to the putative gene promoters (pACRs; within 2 kb upstream of a gene) (Supplementary Fig. 5c-f), consistent with previously reported ATAC-seq data sets (Lu *et al.*, 2017; Sijacic *et al.*, 2018). ~8% of ACRs mapped to distal intergenic genome loci (dACRs) (Supplementary Fig. 5c-f), slightly higher than 5.9% reported recently (Lu *et al.*, 2019). In addition,

14

compared to 16,296 ACRs observed in total using a similar FANS-ATAC-seq approach in a recent report (Lu *et al.*, 2019), we obtained a range of 24,901 to 27,285 total ACRs (Fig. 1c; Supplementary Table 3), also slightly more than the 23,288 total reported elsewhere applying ATAC-seq with INTACT (isolation of nuclei tagged in specific cell types) purified nuclei (Maher *et al.*, 2018). Comparing ACRs enriched in all conditions, we found 10,658 (~ 40% of total ACRs) are shared (Fig. 1c). The remaining 60% unshared ACRs may point to regulatory signals that are specific to each condition.

Among those shared ACRs, pACRs enriched at house-keeping gene loci, such as the *UBQ10* (*POLYUBIQUITIN 10*), show similar patterns in all conditions (Fig. 1d), consistent with the presumed constitutive expression. pACRs enriched at *SNC1* and *SARD1* are similar to those observed in our trial run (Supplementary Fig. 4a,b) and the major peaks of pACRs at these two gene loci under different conditions are similar. We observe additional small pACRs at *SNC1* and increased ACRs at the 3'UTR of *SARD1* upon PTI and 'PTI+ETI' treatment (Fig. 1e,f). Those observations are positively correlated with previous reports that expression of *SARD1* and *SNC1* are upregulated by immune activation (Xia *et al.*, 2013; Ding *et al.*, 2020).

Positive correlation of increased ACRs and expression of defense genes during PTI and 'PTI+ETI'

We reported that some defense genes are induced by both PTI and 'PTI+ETI' by profiling expressions of selected genes (Ding *et al.*, 2020). In this study, we performed genome-wide RNA-seq to study genes induced by PTI and 'PTI+ETI' more extensively (Supplementary Fig. 6a,b). There are 4665 and 5004 upregulated genes during PTI and 'PTI+ETI' compared to the 'No treatment' control, respectively. Among these, 4494 genes are shared by PTI and 'PTI+ETI' (Supplementary Fig. 6c, Supplementary Tables 4). Similarly, there are 5433 downregulated genes shared by PTI and 'PTI+ETI' (Supplementary Fig. 6c). This greatly expands the shared list of genes showing similar regulatory

15

patterns between PTI and 'PTI+ETI' compared to our previous report (Supplementary Fig. 6c,d; Supplementary Tables 5) (Ding *et al.*, 2020). Upregulated genes shared by PTI and 'PTI+ETI' are mostly enriched in gene ontology as defense-related genes or genes in response to stress (Supplementary Fig. 6e,g), whereas downregulated genes shared by both immune activation conditions are enriched with respect to genes involved in photosynthesis (Supplementary Fig. 6f,h). These results indicate a transcriptional reprogramming from photosynthesis to defense activation in Arabidopsis leaves upon activation of both immune conditions. In addition, we identified 3005 genes that are more strongly induced by 'PTI+ETI' compared to PTI alone, and they distribute in Clusters 5, 7 and 9 based on their co-expression pattern (Supplementary Fig. 6d, i-k).

We hypothesized that rapid elevation of gene expression would be correlated with increased chromatin accessibility at these gene loci during immune activation, as active transcription usually requires increased access of DNA-binding proteins such as TFs and transcriptional machineries (Klemm *et al.*, 2019). To test this, we displayed ATAC-seq and corresponding RNA-seq data for well-known defense gene loci (Fig. 2). These were *ISOCHORISMATE SYNTHASE 1* (*ICS1*), *ENHANCED DISEASE SUSCEPTIBILITY 5* (*EDS5*) and *AVRPPHB SUSCEPTIBLE 3* (*PBS3*), genes involved in SA biosynthesis (Wildermuth *et al.*, 2001; Rekhter *et al.*, 2019; Torrens-Spence *et al.*, 2019; Ding and Ding, 2020); and *AGD2-LIKE DEFENSE RESPONSE PROTEIN 1* (*ALD1*), *SAR DEFICIENT 4* (*SARD4*) and *FLAVIN-DEPENDENT MONOOXYGENASE 1* (*FMO1*), genes involved in synthesizing pipecolic acid (Pip) and its derivatives, that contribute to systemic acquired resistance (SAR) and defense priming (Návarová *et al.*, 2012; Ding *et al.*, 2016; Hartmann *et al.*, 2018; Chen *et al.*, 2018). We observed strongly increased ACRs at the promoters of all six selected genes in PTI and 'PTI+ETI' compared to 'No treatment' or Mock treatments (Fig. 2a-f) and increased transcripts of those genes (Fig. 2g-i). This indicates a positive correlation between rapid transcriptional upregulation of selected defense genes and increased ACRs near the corresponding gene loci during activation of PTI and 'PTI+ETI'.

16

Genome-wide assessment of gene regulatory changes during ETI without PTI

Activation of ETI requires effector delivery from a pathogen, so will usually be preceded by PTI (except perhaps for some recognized viruses). Previous studies on ETI usually involve effector delivery from *Pseudomonas sp.* or *Agrobacterium* transient expression, and thus are studies on 'PTI+ETI'. We reported previously an inducible ETI system by expressing AvrRps4^WT^ (SETI^WT^) in which AvrRps4^WT^ is only expressed upon β-estradiol (E2) induced nuclear binding of XVE to the LexA operon (E2:AvrRps4^WT^) (Ngou *et al.*, 2020*b*). This system enables investigation of ETI-specific physiological changes (Ngou *et al.*, 2021).

ETI induced in SETI^WT^ displays similar transcriptional dynamics to that induced by Pf0-1 EtHAn (Ngou *et al.*, 2020*b*). We focused on ETI-specific transcriptional activation; all RNA-seq samples were collected at a relatively early time point of the activation (4 hpi of E2) (Supplementary Fig. 7a) (Ngou *et al.*, 2020*b,a*). To obtain the list of differentially expressed genes (DEGs) during ETI, we compared gene expression profiles in E2-treated SETI^WT^ at 4 hpi (ETI) to those in E2-treated SETI^WT^ at 0 hpi (Control_1) or to those in E2-treated SETI^mut^ at 4 hpi (ETI_mut) (Supplementary Fig. 7a-d; Supplementary Tables 6 and 7). The comparisons of 'ETI vs Control_1' and 'ETI vs ETI_mut' share mostly the same genes in both up- and down-regulation groups (1584 shared upregulated and 1869 shared downregulated genes, respectively) (Supplementary Fig. 7b-d). The number of DEGs in 'ETI vs Control_1' is much more than that in 'ETI vs ETI_mut' (Supplementary Fig. 7b,d). The majority of up- and down-regulated DEGs in 'ETI vs ETI_mut' were shared by 'ETI vs Control_1' (Supplementary Fig. 7c; Supplementary Tables 6). From the gene ontology (GO) enrichment analysis of DEGs in those comparisons, we found the GO term of 'response to wounding' is enriched in DEGs of 'ETI vs Control_1' but not in that of 'ETI vs ETI_mut' (Supplementary Fig. 7e-h). This indicates that both ETI and ETI_mut activate genes that are induced by mechanical wounding via the infiltration process at

17

4 hpi. Thus, comparing ETI to ETI_mut in 'ETI vs ETI_mut' eliminates wounding-induced genes, and reduces background. From these DEGs in 'ETI vs ETI_mut', we found genes mostly enriched in GO terms of 'response to chitin', 'protein phosphorylation' and 'defense response' (Supplementary Fig. 7i-k) (Ngou *et al.*, 2021).

To study the changes in accessible chromatin on the loci of DEGs, we performed FANS-ATAC-seq (Supplementary Fig. 8a). Instead of using E2 treatment at 0 hpi, we use mock-treated sample at 4 hpi as a negative control, imitating the effects from wounding (Supplementary Fig. 8a). We observed consistent genomic distribution patterns of ACRs in all samples (Supplementary Fig. 8b-j; Supplementary Tables 8). To demonstrate ACRs that are specifically induced by ETI compared to all control conditions, we checked the *ICS1* locus in comparison to the house-keeping gene *UBQ10* locus (Fig. 3a,b). We found only ETI induces differential accessible regions (DARs) in the *ICS1* promoter and 3'UTR, but not in the 'No treatment_1' control (Fig. 3a). In contrast *UBQ10* promoter and proximal region are accessible among all treatments (Fig. 3b), therefore we name this type of open chromatin as constitutive accessible chromatin regions (CARs). This is consistent with stable expression of *UBQ10* under all conditions.

Integration of ATAC-seq and mRNA-seq results in PTI, ETI and 'PTI+ETI'

To identify genome-wide DARs that are activated by PTI, ETI and 'PTI+ETI' we normalized the ATAC peaks enriched in PTI, ETI and 'PTI+ETI' treatments compared to corresponding control conditions (Supplementary Fig. 9a-c). We found that DARs become visible at promoters of *ICS1* and *FMO1* as well as the NADPH oxidase encoding *RbohD* in response to the activation of PTI, ETI and 'PTI+ETI' (Fig. 4a), consistent with their upregulated gene expression in these conditions (Supplementary Fig. 6 and 7) (Ngou *et al.*, 2021). We also found that no DARs are observed at *BIK1* locus under PTI, ETI

18

and 'PTI+ETI' (Fig. 4b), though *BIK1* gene expression is induced in all these conditions (Supplementary Fig. 6 and 7) (Ngou *et al.*, 2021). In addition, we observed that DARs at *PEP1 RECEPTOR 2* (*PEPR2*) and *SARD1* loci are only significantly induced by ETI (Fig. 4b), but their gene expression is induced at all immune activation conditions (Supplementary Fig. 6 and 7) (Ngou *et al.*, 2020*a*). This indicates that not all increased DARs activated by different immune systems are positively associated with their upregulated gene expression.

To determine the extent to which activated open chromatin regions from the ATAC-seq analysis are correlated with induced gene expression in all immune conditions we integrated our ATAC-seq data with corresponding mRNA-seq data. We found 1646 gene loci with increased ATAC peaks (DARs) as well as significantly upregulated gene expression (DEGs) in PTI versus 'No treatment', and 1722 such loci in 'PTI+ETI' versus 'No treatment' (Fig. 4c; Supplementary Tables 9). By comparing the intersection of the positively correlated gene loci ('DAR ∩ DEG'), we found substantial overlap (1413 gene loci) between these two conditions (Fig. 4c; Supplementary Tables 9). Comparing 'ETI vs Mock', we found 947 loci showing positive correlation of increased DARs and upregulated DEGs (Fig. 4d; Supplementary Tables 9). The same GO terms are enriched in both 1413 and 947 loci lists (Supplementary Fig. 9c,d; Supplementary Tables 9). Thus, a common set of genes is activated during PTI, ETI and 'PTI+ETI', and transcriptional activation might require chromatin in these gene loci to open up for active transcription events.

To better understand the correlation between DEGs and DARs that are induced by PTI, ETI and 'PTI+ETI', we individually compared upregulated DEGs, DARs and 'DAR∩DEG' that are activated in these conditions compared to corresponding control conditions (Fig.4 e-g; Supplementary Tables 9). We found a large proportion of both upregulated genes and increased DARs are shared by all three immune activation conditions (Fig. 4e,f; Supplementary Tables 9). We then compared PTI, ETI and

'PTI+ETI' upregulated DEGs and DARs ('DAR∩DEG'), and identified 782 gene loci are shared by PTI, ETI and 'PTI+ETI' (Fig. 4g, Supplementary Tables 9). These responses shared by PTI, ETI and 'PTI+ETI' could reveal common transcriptional regulatory mechanism, where a common set of TFs might be required for controlling gene expression.

Transcriptional gene regulatory networks (GRNs) of PTI, ETI and 'PTI+ETI'

Identification of ACRs can assist to determine locations of putative CREs, where transcriptional regulators, especially DNA-binding proteins such as TFs, might bind. To identify regulatory interactions between TF regulators and target genes, gene regulatory networks (GRNs) were delineated through the integration of RNA-Seq, ATAC-Seq and TF motif information (Kulkarni *et al.*, 2018). GRNs at an early time point (4 hpi) upon activation of PTI, ETI and 'PTI+ETI' were constructed, based on motifs enriched for DAR in these conditions. TF binding site mapping data for 1,793 motifs, corresponding to 916 Arabidopsis TFs were used to link specific regulators with putative target genes, based on the motif location in the DAR and the closest gene (Kulkarni *et al.*, 2018). To narrow down the list of TFs, we selected those which showed increased gene expression (log2FC > 1, q-value < 0.01, Supplementary Tables 10). We identified 115, 34 and 133 TFs as regulators in PTI, ETI and 'PTI+ETI', based on the significant enrichment of 210, 73 and 248 motifs in the corresponding DARs (Fig. 5a, Supplementary Tables 10). Comparing regulators between the different conditions reveals that 25 regulators, of which 72% are WRKY TFs, are common to all 3 networks, while 82 regulators are shared between PTI and 'PTI+ETI', corresponding predominantly with WRKY, bHLH and bZIP TFs (Fig. 5b). This result reveals a diversity of TF families is playing an important role in the transcriptional reprogramming of gene expression during the activation of plant immunity.

To assess the biological processes controlled by these different regulators, GO enrichment was performed on each set of target genes, per network and per TF. We found 'response to chitin', 'response to bacterium' and 'response to hypoxia' are the top three GO terms that are commonly enriched in PTI, ETI and 'PTI+ETI' (Fig. 5c, Supplementary Fig. 10, Supplementary Tables 10). Whereas most WRKYs are activated during immune responses independently of whether the activation occurs through surface or intracellular receptors, WRKY65 and WRKY59 are specific to ETI, and the targets of WRKY59 are enriched in 'regulation of cell death' (Fig. 6, Supplementary Fig. 10b). Some examples of TFs implicated by this analysis, some of which have been confirmed in controlling hormone-related processes, are: (1) response to JA and SA in PTI: AtIDD5; (2) response to SA in PTI: KAN2, WRKY33, WRKY45, TGA7, and JKD; (3) SA signaling in ETI: AT5G01380; and (4) response to SA in 'PTI+ETI': KAN2, ANAC029, ANAC046, ABO3, TGA3 and TGA7 (Supplementary Fig. 10). Response to ABA was only observed for 8 WRKY TFs in PTI (WRKY7, 11, 15, 17, 22, 40, 45 and 75), which might be mostly associated with the wounding response. Stronger induction of ETI in addition to PTI might be more dominant to this ABA or wounding-associated transcriptional regulation. Two members of the CAMTA transcription factor family (CAMTA1 and CAMTA3) are exclusively enriched in ETI and were previously characterized as repressors of SA-regulated genes. However, upon pathogen infection CAMTA-mediated repression is alleviated and plant defense genes are expressed (Kidokoro *et al.*, 2017; Kim *et al.*, 2017; Yuan *et al.*, 2018). These results indicate that the function of these CAMTA transcription factors involved in immunity are mediated by intracellular receptors. For PTI there is only one TF exclusive to this condition, CBF2, that regulates a PTI-specific GO term, 'toxin metabolic process'.

The clustering coefficient of a network is a measure of the tendency of the nodes to cluster together, which for GRNs indicates that for specific genes, the incoming regulatory TFs are also controlling each other, suggesting TF crosstalk. The clustering coefficient is significantly higher for PTI and ETI networks than for 'PTI+ETI' and the intersection of PTI, ETI and 'PTI+ETI' (PTI∩ETI∩'PTI+ETI', or 'Set D') (Supplementary Fig. 11). The ETI network stands out having 23 genes with a clustering coefficient of 0.5 or higher, which are controlled by a combination of WRKY TFs (WRKY6, 26, 31, 40, 47 and 70), CAMTA3, HSFB2A and IDD1 (Supplementary Fig. 12). Overall, the inferred networks revealed that both shared and unique regulators are involved in controlling gene expression, with an important role for WRKY TFs controlling the 'response to bacteria' as well as other TFs regulating other hormone-related biological processes. In addition, the tight control of specific target genes by multiple TFs, some also controlling each other, enables investigation into the hierarchy of TF signaling in different types of immunity activation.

Discussion

Our understanding of transcriptional regulation in eukaryotes has been greatly advanced by application of high-throughput sequencing methods to chromatin biology (Meyer and Liu, 2014). Genome-wide chromatin accessibility data for different plant species have demonstrated interesting aspects of mechanisms involved in transcriptional regulation of diverse biological processes (Maher *et al.*, 2018; Sijacic *et al.*, 2018; Potter *et al.*, 2018; Frerichs *et al.*, 2019; Lu *et al.*, 2019; Ricci *et al.*, 2019), but rarely for plant immunity. Several TFs have been implicated in plant innate immunity (Tsuda and Somssich, 2015; Garner *et al.*, 2016). How these TFs function in a regulatory network has remained poorly understood. Here we report chromatin accessibility landscapes that are activated by both cell-surface- and intracellular- immune receptor-mediated immunity (PTI and ETI). There are

22

few studies of ETI in the absence of PTI, and we highlight here the similarity and differences for changes in chromatin accessibility and associated gene expression between these two systems. For those who are interested in PTI or ETI, these datasets comprise a valuable resource for identifying potential novel regulatory components. In addition, these comparative studies document for the first time the similarities and differences of PTI, ETI and 'PTI+ETI', directly demonstrating the interactive relationship between the cell-surface and intracellular immune systems at the transcriptional level.

From the minimum GRNs we constructed here based on our ATAC-seq and RNA-seq results after filtering with selected GO terms, we show that WRKY transcription factors are the predominant players in the GRNs regulating most genes that are activated during both PTI and ETI. However, due to incomplete public data, our GRNs here cannot reflect all regulatory possibilities. For instance, the DNA-binding motifs of some TFs are still not known (O'Malley *et al.*, 2016). In addition, we prioritized upregulated genes in our analysis, and negative regulation of some genes upon TF binding might also play an important role. These networks will be further improved when more data become available.

Another important area of uncertainty is the link between the recruitment of TFs to defense gene promoters and changes in chromatin accessibility. Several working models have been proposed in which chromatin accessibility remodeling is led by the TFs (Klemm *et al.*, 2019). For upregulated DEGs that show increased DARs, the binding of TFs might be correlated with chromatin opening. However, it is challenging to distinguish whether TF binding is cause or consequence of chromatin opening. Some TFs can serve as 'pioneer' TFs to initiate transcription by recruiting 'non-pioneer' TFs, other transcriptional regulators and the RNA polymerase II machinery (Meyer and Liu, 2014; Soufi *et al.*, 2015; Jin *et al.*, 2020). Such 'pioneer' TFs may recruit components that can open the chromatin,

such as histone remodelers (Meyer and Liu, 2014). However more genetic evidence is required to evaluate this hypothesis.

The chromatin accessibility landscapes and implied GRNs reported here provide a snapshot of events during the activation of different immune responses. Transcription, like many other processes, is dynamic, so it is important to profile the changes in chromatin accessibility and corresponding gene expression over a time-course. For instance, our PTI ATAC-seq data were collected at 4 hpi, but PTI-induced transcriptional reprogramming occurs as early as within first thirty minutes post PTI activation (Bjornson *et al.*, 2021); therefore, it is uncertain whether the changes in chromatin accessibility induced by PTI is the cause or effect of the PTI-induced transcriptional changes. With time-series ATAC-seq and RNA-seq data in future studies, we will be able to generate dynamic transcriptional regulatory networks that will provide more insights into transcriptional regulatory mechanisms required for immune activation and for the establishment of disease resistance. Overall, the tools we provide here can also be broadly applied to analyze ATAC-seq and RNA-seq datasets generated from studying any inducible or developmentally regulated system. The network analysis, conducted here with Arabidopsis, can also be compared to network analyses with other plant species when their ATAC-seq and RNA-seq datasets are available, enabling evolutionary comparisons of gene regulatory networks across plant species.

Data availability

All raw reads in this study have been uploaded to the European Nucleotide Archive (ENA) as data repository and can be retrieved through accession number PRJEB34955 and PRJEB38924 for RNA-seq and PRJEB38923 for ATAC-seq. For data reproducibility, all scripts generated in this study, software versions can be found in related GitHub links indicated in the Methods section.

Author contributions

PD and JDGJ conceptualized and designed the research. PD conducted all experiments with assistance from BPMN and SH. PD together with TS, RKS, NMP, WG and CL performed data analyses with assistance from DM, RZ and KV. PD wrote the manuscript with input from all co-authors. All listed authors helped editing and finalizing the manuscript.

Competing interests

The authors declare no competing interests.

References

Asai S, Furzer OJ, Cevik V, Kim DS, Ishaque N, Goritschnig S, Staskawicz BJ, Shirasu K, Jones JDG. 2018. A downy mildew effector evades recognition by polymorphism of expression and subcellular localization. Nature Communications **9**, 5192.

Bacete L, Mélida H, Miedes E, Molina A. 2018. Plant cell wall-mediated immunity: cell wall changes trigger disease resistance responses. The Plant Journal: for Cell and Molecular Biology **93**, 614–636.

Berriri S, Gangappa SN, Kumar SV. 2016. SWR1 Chromatin-Remodeling Complex Subunits and H2A.Z Have Non-overlapping Functions in Immunity and Gene Regulation in Arabidopsis. Molecular Plant **9**, 1051–1065.

van der Biezen EA, Freddie CT, Kahn K, Parker JE, Jones JDG. 2002. Arabidopsis RPP4 is a member of the RPP5 multigene family of TIR-NB-LRR genes and confers downy mildew resistance through multiple signalling components. The Plant Journal: for Cell and Molecular Biology **29**, 439–451.

Bjornson M, Pimprikar P, Nürnberger T, Zipfel C. 2021. The transcriptional landscape of Arabidopsis thaliana pattern-triggered immunity. Nature Plants **7**, 579–586.

Bray NL, Pimentel H, Melsted P, Pachter L. 2016. Near-optimal probabilistic RNA-seq quantification. Nature Biotechnology **34**, 525–527.

Buenrostro JD, Giresi PG, Zaba LC, Chang HY, Greenleaf WJ. 2013. Transposition of native chromatin for fast and sensitive epigenomic profiling of open chromatin, DNA-binding proteins and nucleosome position. Nature Methods **10**, 1213–1218.

Buenrostro JD, Wu B, Chang HY, Greenleaf WJ. 2015. ATAC-seq: A Method for Assaying Chromatin Accessibility Genome-Wide. Current Protocols in Molecular Biology **109**, 21.29.1-21.29.9.

27

Chen Y-C, Holmes EC, Rajniak J, Kim J-G, Tang S, Fischer CR, Mudgett MB, Sattely ES. 2018. N-hydroxy-pipecolic acid is a mobile metabolite that induces systemic disease resistance in Arabidopsis. Proceedings of the National Academy of Sciences of the United States of America **115**, E4920–E4929.

Chen W, Zhu Q, Liu Y, Zhang Q. 2017. Chromatin remodeling and plant immunity. Advances in protein chemistry and structural biology **106**, 243–260.

Choi HW, Klessig DF. 2016. DAMPs, MAMPs, and NAMPs in plant innate immunity. BMC Plant Biology **16**, 232.

Conway JR, Lex A, Gehlenborg N. 2017. UpSetR: an R package for the visualization of intersecting sets and their properties. Bioinformatics **33**, 2938–2940.

Ding P, Ding Y. 2020. Stories of salicylic acid: A plant defense hormone. Trends in Plant Science **25**, 549–565.

Ding P, Ngou BPM, Furzer OJ, Sakai T, Shrestha RK, MacLean D, Jones JDG. 2020. High-resolution expression profiling of selected gene sets during plant immune activation. Plant Biotechnology Journal **18**, 1610–1619.

Ding P, Rekhter D, Ding Y, *et al.* 2016. Characterization of a pipecolic acid biosynthesis pathway required for systemic acquired resistance. The Plant Cell **28**, 2603–2615.

Dong OX, Ao K, Xu F, *et al.* 2018. Individual components of paired typical NLR immune receptors are regulated by distinct E3 ligases. Nature Plants **4**, 699–710.

Frerichs A, Engelhorn J, Altmüller J, Gutierrez-Marcos J, Werr W. 2019. Specific chromatin changes mark lateral organ founder cells in the Arabidopsis inflorescence meristem. Journal of Experimental Botany **70**, 3867–3879.

Frith MC, Li MC, Weng Z. 2003. Cluster-Buster: Finding dense clusters of motifs in DNA sequences.

Nucleic Acids Research **31**, 3666–3668.

Garner CM, Kim SH, Spears BJ, Gassmann W. 2016. Express yourself: Transcriptional regulation of plant innate immunity. Seminars in Cell & Developmental Biology **56**, 150–162.

Grant CE, Bailey TL, Noble WS. 2011. FIMO: scanning for occurrences of a given motif. Bioinformatics **27**, 1017–1018.

Guo W, Tzioutziou NA, Stephen G, Milne I, Calixto CP, Waugh R, Brown JWS, Zhang R. 2020. 3D RNA-seq: a powerful and flexible tool for rapid and accurate differential expression and alternative splicing analysis of RNA-seq data for biologists. RNA Biology, 1–14.

Hammond-Kosack KE, Jones JDG. 1997. PLANT DISEASE RESISTANCE GENES. Annual review of plant physiology and plant molecular biology **48**, 575–607.

Hartmann M, Zeier T, Bernsdorff F, *et al*. 2018. Flavin Monooxygenase-Generated N-Hydroxypipecolic Acid Is a Critical Element of Plant Systemic Immunity. Cell **173**, 456–469.e16.

Hillmer RA, Tsuda K, Rallapalli G, Asai S, Truman W, Papke MD, Sakakibara H, Jones JDG, Myers CL, Katagiri F. 2017. The highly buffered Arabidopsis immune signaling network conceals the functions of its components. PLoS Genetics **13**, e1006639.

Jin R, Klasfeld S, Garcia MF, Xiao J, Han S-K, Konkol A, Zhu Y, Wagner D. 2020. LEAFY is a pioneer transcription factor and licenses cell reprogramming to floral fate. BioRxiv.

Johnson KCM, Xia S, Feng X, Li X. 2015. The Chromatin Remodeler SPLAYED Negatively Regulates SNC1-Mediated Immunity. Plant & Cell Physiology **56**, 1616–1623.

Jones JDG, Dangl JL. 2006. The plant immune system. Nature **444**, 323–329.

Kidd BN, Edgar CI, Kumar KK, Aitken EA, Schenk PM, Manners JM, Kazan K. 2009. The mediator complex subunit PFT1 is a key regulator of jasmonate-dependent defense in Arabidopsis. The Plant

Cell **21**, 2237–2252.

Kidokoro S, Yoneda K, Takasaki H, Takahashi F, Shinozaki K, Yamaguchi-Shinozaki K. 2017. Different Cold-Signaling Pathways Function in the Responses to Rapid and Gradual Decreases in Temperature. The Plant Cell **29**, 760–774.

Kim YS, An C, Park S, Gilmour SJ, Wang L, Renna L, Brandizzi F, Grumet R, Thomashow MF. 2017. CAMTA-Mediated Regulation of Salicylic Acid Immunity Pathway Genes in Arabidopsis Exposed to Low Temperature and Pathogen Infection. The Plant Cell **29**, 2465–2477.

Kim D, Pertea G, Trapnell C, Pimentel H, Kelley R, Salzberg SL. 2013. TopHat2: accurate alignment of transcriptomes in the presence of insertions, deletions and gene fusions. Genome Biology **14**, R36.

Klemm SL, Shipony Z, Greenleaf WJ. 2019. Chromatin accessibility and the regulatory epigenome. Nature Reviews. Genetics **20**, 207–220.

Kulkarni SR, Jones DM, Vandepoele K. 2019. Enhanced Maps of Transcription Factor Binding Sites Improve Regulatory Networks Learned from Accessible Chromatin Data. Plant Physiology **181**, 412–425.

Kulkarni SR, Vaneechoutte D, Van de Velde J, Vandepoele K. 2018. TF2Network: predicting transcription factor regulators and gene regulatory networks in Arabidopsis using publicly available binding site information. Nucleic Acids Research **46**, e31.

Langmead B, Salzberg SL. 2012. Fast gapped-read alignment with Bowtie 2. Nature Methods **9**, 357–359.

Law CW, Chen Y, Shi W, Smyth GK. 2014. voom: Precision weights unlock linear model analysis tools for RNA-seq read counts. Genome Biology **15**, R29.

Li H, Handsaker B, Wysoker A, Fennell T, Ruan J, Homer N, Marth G, Abecasis G, Durbin R, 1000 Genome Project Data Processing Subgroup. 2009. The Sequence Alignment/Map format and

SAMtools. Bioinformatics **25**, 2078–2079.

Li B, Meng X, Shan L, He P. 2016. Transcriptional Regulation of Pattern-Triggered Immunity in Plants. Cell Host & Microbe **19**, 641–650.

Lu Z, Hofmeister BT, Vollmers C, DuBois RM, Schmitz RJ. 2017. Combining ATAC-seq with nuclei sorting for discovery of cis-regulatory regions in plant genomes. Nucleic Acids Research **45**, e41.

Lu Z, Marand AP, Ricci WA, Ethridge CL, Zhang X, Schmitz RJ. 2019. The prevalence, evolution and chromatin signatures of plant regulatory elements. Nature Plants **5**, 1250–1259.

Maher KA, Bajic M, Kajala K, *et al.* 2018. Profiling of Accessible Chromatin Regions across Multiple Plant Species and Cell Types Reveals Common Gene Regulatory Principles and New Control Modules. The Plant Cell **30**, 15–36.

Meyer CA, Liu XS. 2014. Identifying and mitigating bias in next-generation sequencing methods for chromatin biology. Nature Reviews. Genetics **15**, 709–721.

Návarová H, Bernsdorff F, Döring A-C, Zeier J. 2012. Pipecolic acid, an endogenous mediator of defense amplification and priming, is a critical regulator of inducible plant immunity. The Plant Cell **24**, 5123–5141.

Ngou BPM, Ahn H-K, Ding P, Jones JD. 2020*a*. Mutual Potentiation of Plant Immunity by Cell-surface and Intracellular Receptors. BioRxiv.

Ngou BPM, Ahn H-K, Ding P, Jones JDG. 2021. Mutual potentiation of plant immunity by cell-surface and intracellular receptors. Nature.

Ngou BPM, Ahn H-K, Ding P, Redkar A, Brown H, Ma Y, Youles M, Tomlinson L, Jones JDG. 2020*b*. Estradiol-inducible AvrRps4 expression reveals distinct properties of TIR-NLR-mediated effector-triggered immunity. Journal of Experimental Botany **71**, 2186–2197.

31

O'Malley RC, Huang S-SC, Song L, Lewsey MG, Bartlett A, Nery JR, Galli M, Gallavotti A, Ecker JR. 2016. Cistrome and epicistrome features shape the regulatory DNA landscape. Cell **166**, 1598.

Patro R, Duggal G, Love MI, Irizarry RA, Kingsford C. 2017. Salmon provides fast and bias-aware quantification of transcript expression. Nature Methods **14**, 417–419.

Potter KC, Wang J, Schaller GE, Kieber JJ. 2018. Cytokinin modulates context-dependent chromatin accessibility through the type-B response regulators. Nature Plants **4**, 1102–1111.

Quinlan AR, Hall IM. 2010. BEDTools: a flexible suite of utilities for comparing genomic features. Bioinformatics **26**, 841–842.

Raudvere U, Kolberg L, Kuzmin I, Arak T, Adler P, Peterson H, Vilo J. 2019. g:Profiler: a web server for functional enrichment analysis and conversions of gene lists (2019 update). Nucleic Acids Research **47**, W191–W198.

Rekhter D, Lüdke D, Ding Y, Feussner K, Zienkiewicz K, Lipka V, Wiermer M, Zhang Y, Feussner I. 2019. Isochorismate-derived biosynthesis of the plant stress hormone salicylic acid. Science **365**, 498–502.

Ricci WA, Lu Z, Ji L, *et al.* 2019. Widespread long-range cis-regulatory elements in the maize genome. Nature Plants **5, 1237–1249.

Risso D, Ngai J, Speed TP, Dudoit S. 2014. Normalization of RNA-seq data using factor analysis of control genes or samples. Nature Biotechnology **32**, 896–902.

Ritchie ME, Phipson B, Wu D, Hu Y, Law CW, Shi W, Smyth GK. 2015. limma powers differential expression analyses for RNA-sequencing and microarray studies. Nucleic Acids Research **43**, e47.

Robinson MD, Oshlack A. 2010. A scaling normalization method for differential expression analysis of RNA-seq data. Genome Biology **11**, R25.

32

Robinson JT, Thorvaldsdóttir H, Winckler W, Guttman M, Lander ES, Getz G, Mesirov JP. 2011. Integrative genomics viewer. Nature Biotechnology **29**, 24–26.

Saucet SB, Ma Y, Sarris PF, Furzer OJ, Sohn KH, Jones JDG. 2015. Two linked pairs of Arabidopsis TNL resistance genes independently confer recognition of bacterial effector AvrRps4. Nature Communications **6**, 6338.

Schmid M, Davison TS, Henz SR, Pape UJ, Demar M, Vingron M, Schölkopf B, Weigel D, Lohmann JU. 2005. A gene expression map of Arabidopsis thaliana development. Nature Genetics **37**, 501–506.

Sijacic P, Bajic M, McKinney EC, Meagher RB, Deal RB. 2018. Changes in chromatin accessibility between Arabidopsis stem cells and mesophyll cells illuminate cell type-specific transcription factor networks. The Plant Journal: for Cell and Molecular Biology **94**, 215–231.

Sohn KH, Segonzac C, Rallapalli G, Sarris PF, Woo JY, Williams SJ, Newman TE, Paek KH, Kobe B, Jones JDG. 2014. The nuclear immune receptor RPS4 is required for RRS1SLH1-dependent constitutive defense activation in Arabidopsis thaliana. PLoS Genetics **10**, e1004655.

Sohn KH, Zhang Y, Jones JDG. 2009. The Pseudomonas syringae effector protein, AvrRPS4, requires in planta processing and the KRVY domain to function. The Plant Journal: for Cell and Molecular Biology **57**, 1079–1091.

Soufi A, Garcia MF, Jaroszewicz A, Osman N, Pellegrini M, Zaret KS. 2015. Pioneer transcription factors target partial DNA motifs on nucleosomes to initiate reprogramming. Cell **161**, 555–568.

Staal J, Kaliff M, Dewaele E, Persson M, Dixelius C. 2008. RLM3, a TIR domain encoding gene involved in broad-range immunity of Arabidopsis to necrotrophic fungal pathogens. The Plant Journal: for Cell and Molecular Biology **55**, 188–200.

Sun T, Zhang Y, Li Y, Zhang Q, Ding Y, Zhang Y. 2015. ChIP-seq reveals broad roles of SARD1 and

CBP60g in regulating plant immunity. Nature Communications **6**, 10159.

Thomas WJ, Thireault CA, Kimbrel JA, Chang JH. 2009. Recombineering and stable integration of the Pseudomonas syringae pv. syringae 61 hrp/hrc cluster into the genome of the soil bacterium Pseudomonas fluorescens Pf0-1. The Plant Journal: for Cell and Molecular Biology **60**, 919–928.

Torrens-Spence MP, Bobokalonova A, Carballo V, Glinkerman CM, Pluskal T, Shen A, Weng J-K. 2019. PBS3 and EPS1 Complete Salicylic Acid Biosynthesis from Isochorismate in Arabidopsis. Molecular Plant **12**, 1577–1586.

Tsompana M, Buck MJ. 2014. Chromatin accessibility: a window into the genome. Epigenetics & Chromatin **7**, 33.

Tsuda K, Somssich IE. 2015. Transcriptional networks in plant immunity. The New Phytologist **206**, 932–947.

Walley JW, Rowe HC, Xiao Y, Chehab EW, Kliebenstein DJ, Wagner D, Dehesh K. 2008. The chromatin remodeler SPLAYED regulates specific stress signaling pathways. PLoS Pathogens **4**, e1000237.

Wang L, Tsuda K, Truman W, Sato M, Nguyen LV, Katagiri F, Glazebrook J. 2011. CBP60g and SARD1 play partially redundant critical roles in salicylic acid signaling. The Plant Journal: for Cell and Molecular Biology **67**, 1029–1041.

Wildermuth MC, Dewdney J, Wu G, Ausubel FM. 2001. Isochorismate synthase is required to synthesize salicylic acid for plant defence. Nature **414**, 562–565.

Xia S, Cheng YT, Huang S, _et al._ 2013. Regulation of transcription of nucleotide-binding leucine-rich repeat-encoding genes SNC1 and RPP4 via H3K4 trimethylation. Plant Physiology **162**, 1694–1705.

Yu G, Wang L-G, He Q-Y. 2015. ChIPseeker: an R/Bioconductor package for ChIP peak annotation, comparison and visualization. Bioinformatics **31**, 2382–2383.

Yuan P, Du L, Poovaiah BW. 2018. Ca2+/Calmodulin-Dependent AtSR1/CAMTA3 Plays Critical Roles in Balancing Plant Growth and Immunity. International Journal of Molecular Sciences **19**.

Zhang R, Calixto CPG, Marquez Y, *et al.* 2017. A high quality Arabidopsis transcriptome for accurate transcript-level analysis of alternative splicing. Nucleic Acids Research **45**, 5061–5073.

Zhang Y, Goritschnig S, Dong X, Li X. 2003. A gain-of-function mutation in a plant disease resistance gene leads to constitutive activation of downstream signal transduction pathways in suppressor of npr1-1, constitutive 1. The Plant Cell **15**, 2636–2646.

Zhang Y, Liu T, Meyer CA, *et al.* 2008. Model-based analysis of ChIP-Seq (MACS). Genome Biology **9**, R137.

Zhang Y, Xu S, Ding P, *et al.* 2010. Control of salicylic acid synthesis and systemic acquired resistance by two members of a plant-specific family of transcription factors. Proceedings of the National Academy of Sciences of the United States of America **107**, 18220–18225.

Zhou C, Zhang L, Duan J, Miki B, Wu K. 2005. HISTONE DEACETYLASE19 is involved in jasmonic acid and ethylene signaling of pathogen response in Arabidopsis. The Plant Cell **17**, 1196–1204.

Zhu Z, Xu F, Zhang Y, Cheng YT, Wiermer M, Li X, Zhang Y. 2010. Arabidopsis resistance protein SNC1 activates immune responses through association with a transcriptional corepressor. Proceedings of the National Academy of Sciences of the United States of America **107**, 13960–13965.

Zou B, Sun Q, Zhang W, Ding Y, Yang D-L, Shi Z, Hua J. 2017. The Arabidopsis Chromatin-Remodeling Factor CHR5 Regulates Plant Immune Responses and Nucleosome Occupancy. Plant & Cell Physiology **58**, 2202–2216.

Figure 1
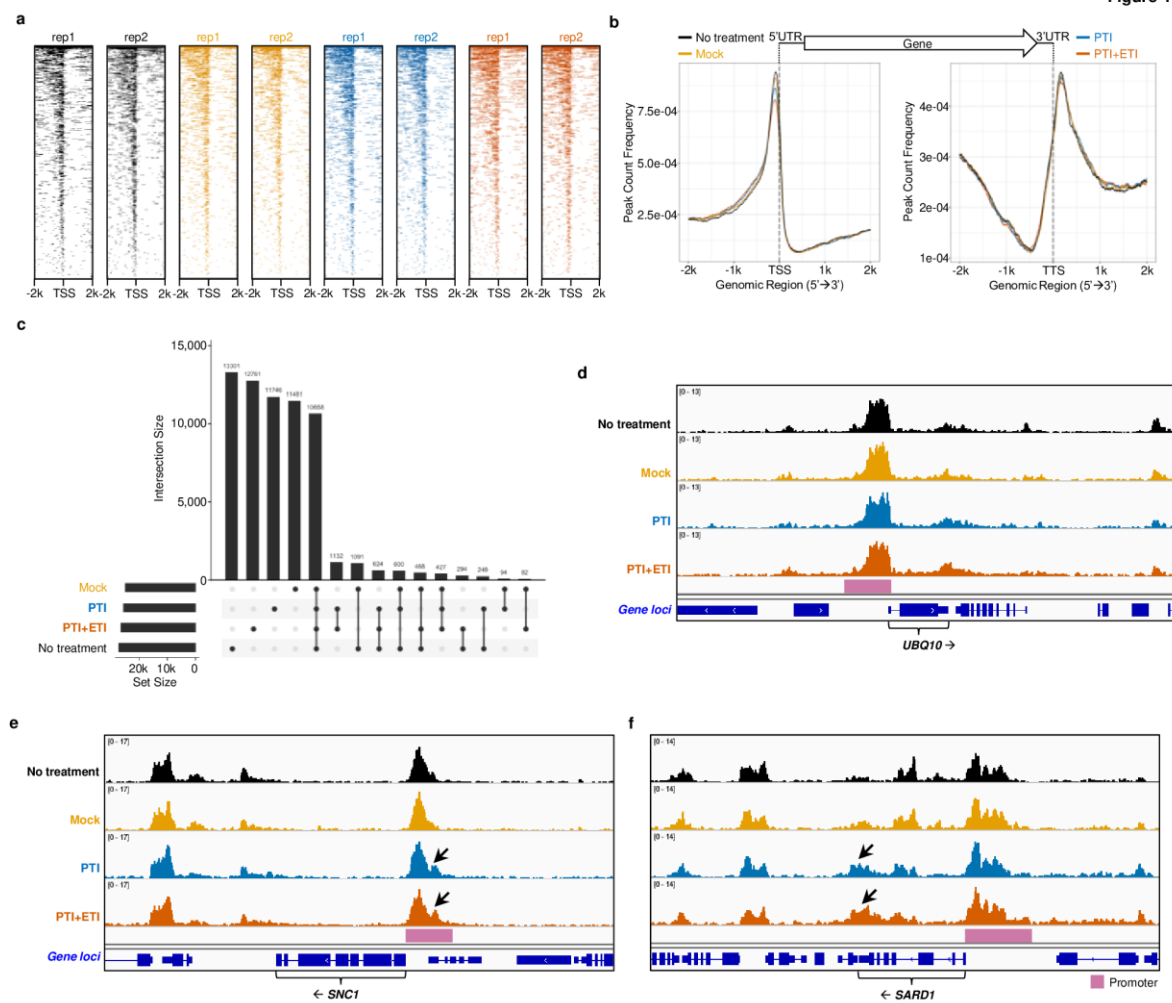
Figure 1. Interrogation of chromatin landscapes activated by PTI and 'PTI+ETI'.
(a) Heatmaps showing the distribution of accessible regions around the TSS identified by FANS-ATAC-seq in two biological replicates (rep) under four different conditions. Accessible regions are mapped to 2,000 bp upstream (-2k) or downstream (2k) of TSS as the center. 'No treatment', Mock, PTI and 'PTI+ETI' are indicated in black, orange, blue and vermillion, respectively (same color codes apply to the same set of treatments in the rest of this study). **(b)** Distribution of accessible regions around the TSS (left panel) and TTS (right panel) identified from FANS-ATAC-seq with the mean peak counts from two biological replicates indicated in (a). The center of accessible regions was used to produce the distribution plots. **(c)** An UpSet plot showing the relationships of accessible regions enriched under four different conditions indicated in (a) and (b). 'Intersection Size' indicates either condition specific accessible regions or shared accessible regions under different combinations of condition comparisons. 'Set Size' indicates the aggregates or total number of accessible regions found under each condition. **(d-f)** Genome browser views of ATAC-seq-indicated chromatin accessibility changes occurring near selected gene loci under different conditions. Gene symbols are labeled for the corresponding gene loci, (d) *UBQ10*, (e) *SNC1* and (f) *SARD1*. The protein coding strand is indicated in black arrow placed next to the gene symbol. The reddish-purple bars next to each gene loci indicate their putative promoter regions.
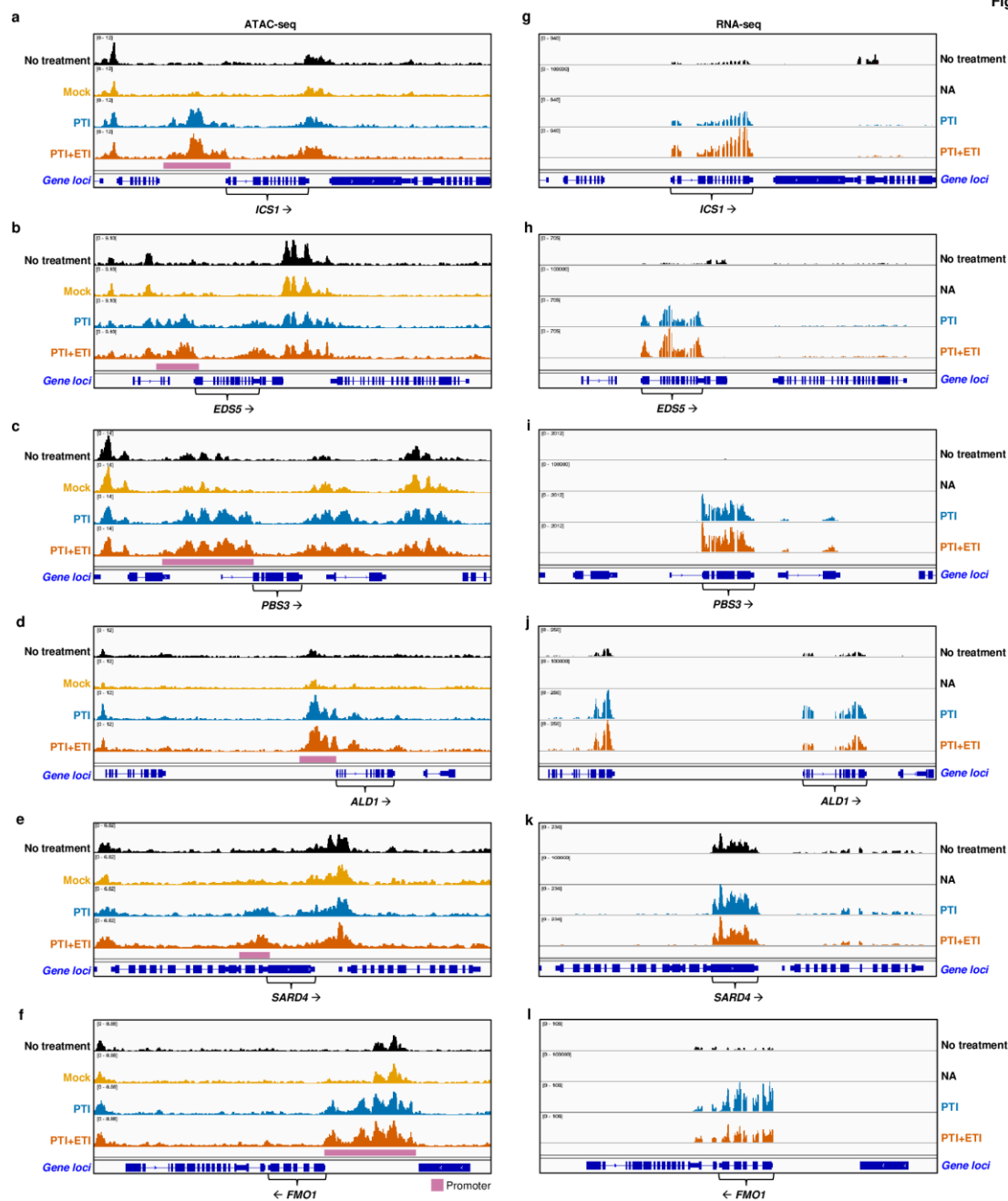**Related supplementary information:**
Supplementary Fig. 5
Supplementary Tables 2 and 3

Figure 2

Figure 2. Integration of ATAC-seq with RNA-seq for genes activated by PTI and 'PTI+ETI'

(**a-f**) and (**g-i**) Genome browser views of ATAC-seq and RNA-seq on indicated gene loci under different conditions. (**a**) and (**g**) are date for *ICS1* locus. (**b**) and (**h**) are date for *EDS5* locus. (**c**) and (**i**) are date for *PBS3* locus. (**d**) and (**j**) are date for *ALD1* locus. (**e**) and (**k**) are date for *SARD4* locus. (**f**) and (**l**) are date for *FMO1* locus. *ICS1*, *EDS5* and *PBS3* are genes encoding enzymes that are required for the biosynthesis of a defense hormone, salicylic acid (SA) in the isochorismate pathway. *ALD1*, *SARD4* and *FMO1* are enzyme encoding genes involved in the biosynthesis of a secondary metabolite, N-hydroxy pipecolic acid (NHP) that are required to initiate systemic acquired resistance in plants. ATAC-seq data contain the same four conditions as shown in Figure 1, whereas the data point of Mock treatment is absent in RNA-seq data (NA). ATAC-seq and RNA-seq data points with the same corresponding labels indicate they were collected under exactly the same conditions (see more details in Methods).
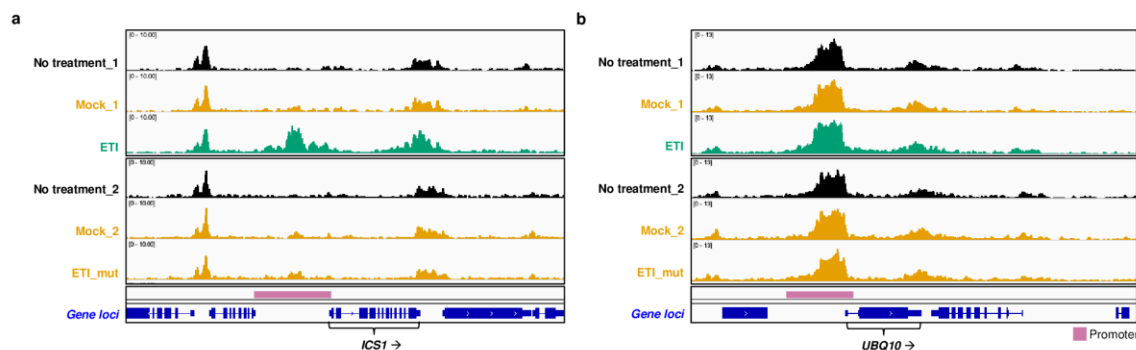
Related supplementary information:

Supplementary Fig. 6

Supplementary Tables 4 and 5

Figure 3

Figure 3. Characterization of chromatin accessible regions activated by ETI

(**a**) and (**b**) Genome browser views of chromatin accessible regions on selected gene loci under different conditions, including ETI. 'No treatment_1' and 'No treatment_2' are colored in black. Mock_1, Mock_2 and ETI_mut are colored in orange. ETI is colored in bluish green. Same color codes apply to the same corresponding conditions in the rest of this study. Gene symbols are labeled for the corresponding gene loci, (a) *ICS1* and (b) *UBQ10*. The protein coding strand is indicated in black arrow placed next to the gene symbol. The reddish-purple bars next to each gene loci indicate their putative promoter regions.
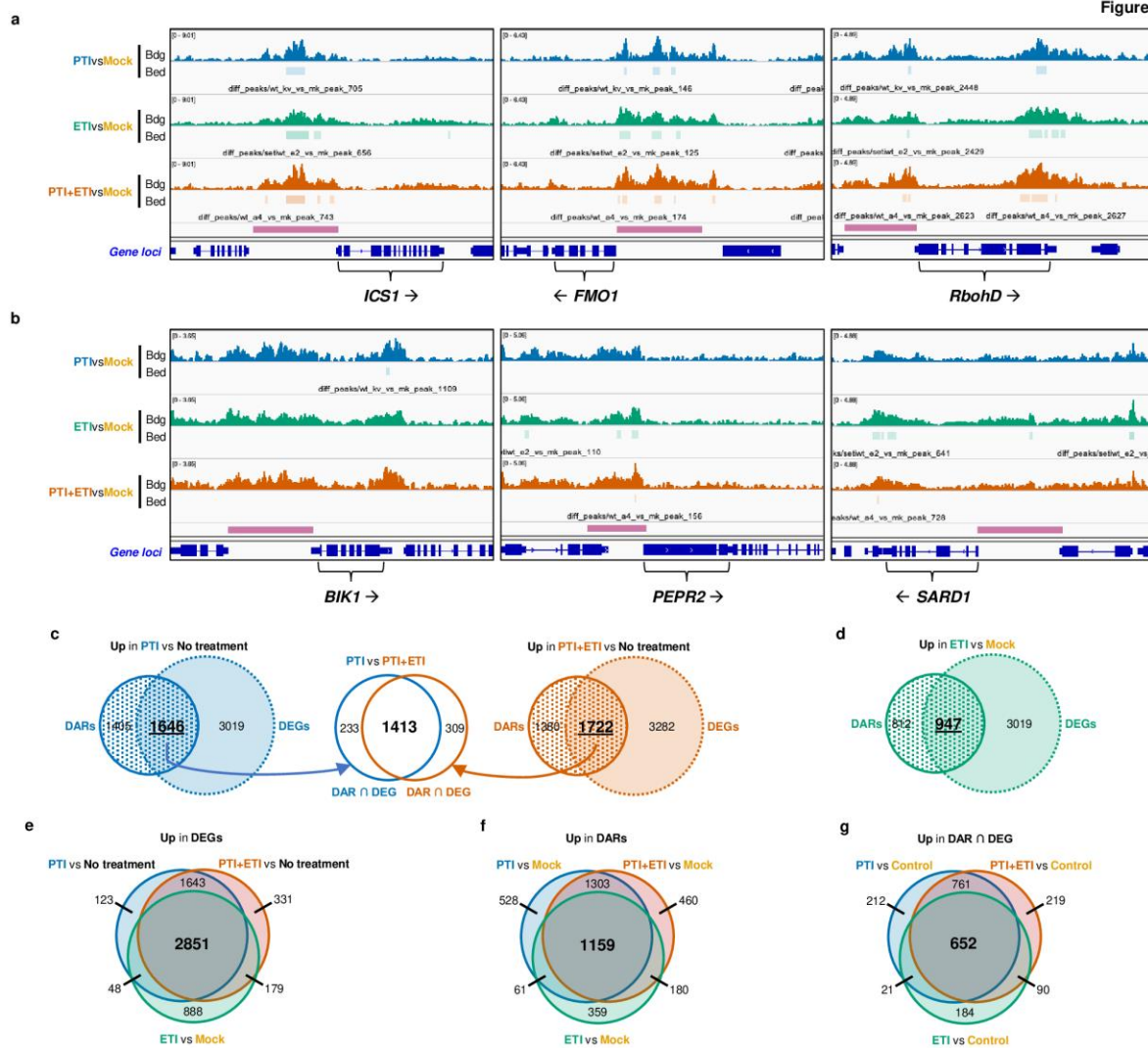
Related supplementary information:

Supplementary Fig. 8
Supplementary Tables 8

Figure 4

Figure 4. Determining chromatin accessibility changes and changes in gene expressions activated by PTI, ETI and 'PTI+ETI'

(a) and (b) Genome browser views of differential accessible chromatin regions (ACRs) near genes that are transcriptionally upregulated in PTI, ETI and 'PTI+ETI' compared to Mock treatments. (a) Gene loci (*ICS1*, *FMO1* and *RbohD*) with increased ACRs in all indicated conditions. (b) Gene loci either have no increased ACRs in all conditions (*BIK1*) or only show increased ACRs in ETI (*PEPR2* and *SARD1*). Other labels follow same keys indicated in Figure 1 to 3. (c) Integration of differential accessible regions (DARs) and differential expression genes (DEGs) between PTI and 'PTI+ETI'. There the DARs indicate the nearest gene loci. The Venn diagrams on the left or right sides show upregulated DARs (circle with dotted pattern) and DEGs (dashed circle with color filled) in PTI (blue, left) or 'PTI+ETI' (vermillion, right) compared to 'No treatment' controls. Shared gene loci with both DARs and DEGs (intersection area in the Venn diagrams, or 'DAR ∩ DEG') from PTI (n = 1635) and 'PTI+ETI' (n = 1722) were compared again in the Venn diagram in the middle. (d) Integration of DARs and DEGs in ETI. The Venn diagram (bluish green) shows upregulated DARs (circle with dotted pattern) and DEGs (dashed circle with color filled) in ETI compared to Mock controls. (e) Comparisons of upregulated DEGs in PTI, ETI and 'PTI+ETI' compared to corresponding negative controls ('No treatment' or Mock). (f) Comparisons of upregulated DARs in PTI, ETI and 'PTI+ETI' compared to corresponding negative controls ('No treatment' or Mock). (g) Comparisons of upregulated 'DAR ∩ DEG' in PTI, ETI and 'PTI+ETI' compared to Controls ('No treatment' or Mock).
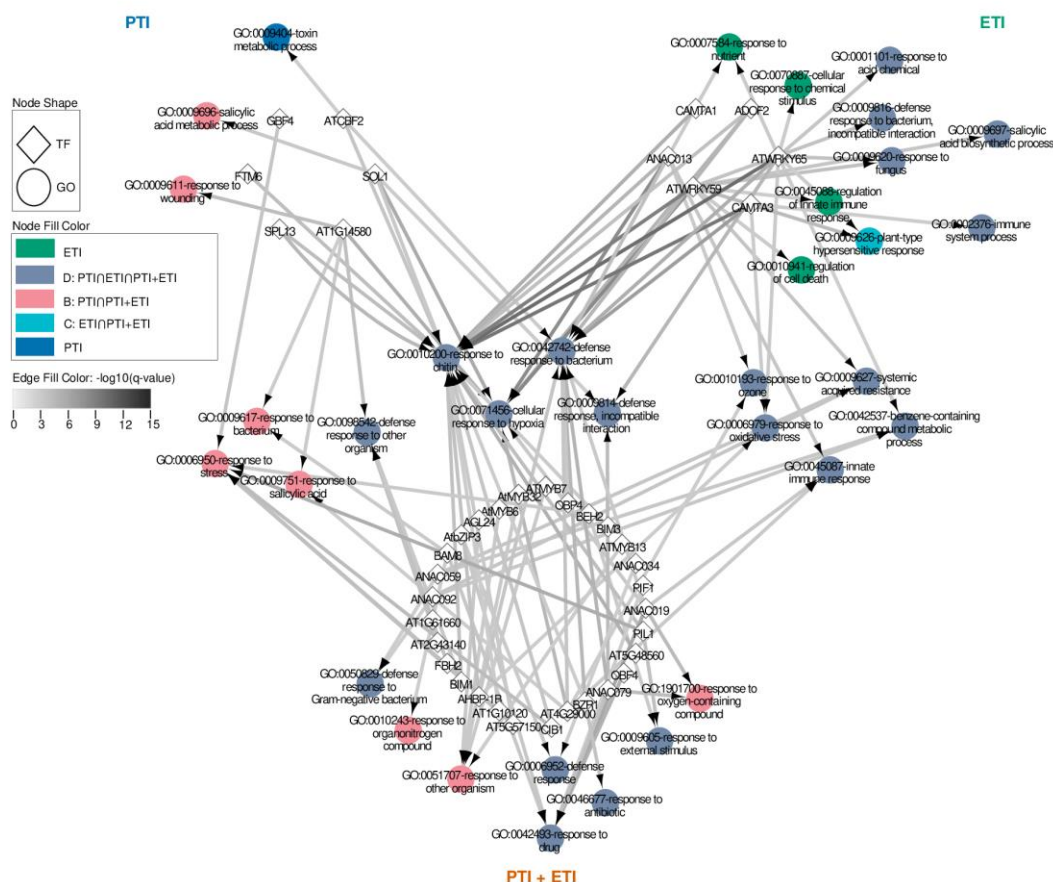
Related supplementary information:
Supplementary Fig. 7, 8 and 9
Supplementary Tables 7, 8 and 9

Figure 5. Overview of regulatory TFs across the different gene regulatory networks.
(a) Venn diagram showing shared and unique TFs across the different networks inferred for each condition. (b) Heatmap with the number of TF family members in each of the Venn diagram sets, as indicated by the coloring of each cell. TFs that are specific to PTI, ETI and 'PTI+ETI' are highlighted with corresponding color code. (c) Heatmap displaying presence or absence of GO terms enrichment in each of the Venn diagram sets. Numbers at the right indicate the number of TFs showing GO enrichment. TFs that are specific to ETI are enriched in 'plant-type hypersensitive response' and 'regulation of cell death' (in blueish green).

Related supplementary information:
Supplementary Fig. 10 and 11
Supplementary Tables 10

43

Figure 6

Figure 6. TF-GO term network for condition-specific TFs

Network diagram with the TFs specific for each condition 'SMRI', 'ETI' and 'PTI+ETI' organized in circles linked to the GO terms enriched in the putative target genes they control. The GO terms are colored according to whether they are exclusive of any specific condition or if they belong in any of the possible intersections of the conditions. The GO terms controlled by TFs exclusive of one condition are in the most outer parts. The GO terms controlled by TFs exclusive of two and three conditions are located closer to the center and in the center, respectively. Note there are not GO terms shared between TFs of PTI and ETI. Also, there are no GO terms that are exclusive of 'PTI+ETI' and 'PTI ∩ ETI' because none of them are controlled by PTI, ETI or 'PTI+ETI' exclusive TFs.

Related supplementary information:

Supplementary Fig. 12

Supplementary Tables 10

44